Materials Science in Semiconductor Processing 151 (2022) 107014

Contents lists available at ScienceDirect

Materials Science in Semiconductor Processing

journal homepage: www.elsevier.com/locate/mssp

On downscaling of the tantalum oxides from three to zero dimensions

Alia Jabeen [a], Mohammad Alkhedher [b], Abdul Majid [a,*], Najam Al Hassan [c]

[a] Department of Physics, University of Gujrat, Gujrat, Pakistan
[b] Mechanical and Industrial Engineering Department, Abu Dhabi University, Abu Dhabi, United Arab Emirates
[c] Department of Physics, Hazara University, Mansehra, KPK, Pakistan

ARTICLE INFO

Keywords:
3D metal oxides
2D metal oxides
1D metal oxides
0D metal oxides
Density functional theory
Formation energy analysis
Tantalum oxides
Structural and electronic properties
Nanotechnology

ABSTRACT

Considering the recent interests in device miniaturization prompted by developments in nanotechnology, study of changes in physical properties of electronic materials upon downscaling to lower dimensions has become more important. This study is aimed at investigating the structural and electronic properties of the tantalum oxides (TaO, TaO_2, Ta_2O_3, TaO_3) in the bulk and lower dimensions of slab, chains and clusters. The predictions pointed out that *TaO*, TaO_2 and Ta_2O_3 prefer to crystallize in bulk whereas TaO_3 stabilizes in form of clusters. The bulk, slab, chains and clusters of TaO exhibit metallic character due to d-electrons at Fermi level. The bulk, slab and clusters of TaO_2 offers the metallic character due to the presence of major contribution of Ta-d states at Fermi level, while the chains appeared as narrow-gap semiconductor which points to a transition from metallic to semiconducting character on downscaling. The bulk and chains of TaO_3 exhibited metallic behavior due to presence of p-states on Fermi level, while the clusters are semiconductors having band gap 2.6 eV. Ta_2O_3 in bulk, slab and chains show metallic character due to presence of d-states of Ta at Fermi level, while the clusters possess the semiconducting nature. In general, the transition from metallic to semiconducting character is observed upon the downscaling. This study gives the valuable predictions for the future usage of these materials in several electronic applications and devices.

1. Introduction

The exploration of new materials exhibiting required physical properties for application in future devices is currently a hot research topic. Nanotechnology, an emerging multidisciplinary field of science, offers nanoscale materials for utilization in several devices and daily life applications [1,2]. The electronic materials, when down scaled to about one billionth of a meter, exhibits completely different properties that are not present in their bulk analogue. The experimental understanding and description of the scientific behavior associated with nanomaterial needs out-of-the-box approach. Quantum physics is helpful to understand the behavior of these materials owing to atypical aspects associated with the magnetism, energetics, transport, and structural evolution, reactivity with the external world and the interaction with light. The reported literature has been very helpful to shed light on properties of known functional nanomaterials that has opened access to several applications but still more work is needed in this regard.

The nanomaterials are down scaled version of the bulk materials. In general, band gap and surface-to-volume ratio of materials increases upon downscalling which opens gateway to variety of new applications in electronics, solar cells, batteries, sensors, medicine, communication, biotechnology etc. The nanomaterials are classified into four classes on the basis of their dimensionality that is 3D, 2D, 1D and OD. In 3D materials, the motion of particles are not confined/quantized in any of the direction and they are free to move within the material [3]. The 2D materials including thin films, nano-slabs [4,5] nano-plates, nanosheets and nanocomposites [6] etc. have shown shape-dependent characteristics and thus have grasped considerable attention [7]. The applications of 2D materials in optoelectronics [8,9], Photodetectors [10] spintronics [11], catalysts [12,13], photocatalysis [14,15]as well in devices like FET [12,16–18], LED's, gas-sensing [12,16], and energy storage devices have been established [19]. In addition to this, owing to the periodic configuration and low dimensionality, the two-dimensional (2D) materials exhibit the electron transmission and large surface area due to which these materials offer excellent adsorption and high elasticity. The 2D materials in high crystal quality are now synthesized through several methods like CVD [20], vacuum arc deposition [21], microwave assisted chemistry approaches and cathodic magnetron sputtering etc. The 1D materials involve confinement of the holes as well as electrons along a line and thus exhibit diverse electronic as well as optical properties. The

* Corresponding author.
E-mail address: abdulmajid40@yahoo.com (A. Majid).

https://doi.org/10.1016/j.mssp.2022.107014
Received 15 March 2022; Received in revised form 27 July 2022; Accepted 31 July 2022
Available online 9 August 2022

decrease in size of bulk materials close to their Bohr radius produces 0D materials like clusters, quantum dots and spheres in which motion of the carriers are completely confined [22,23]. Such quantized energy levels in these materials are primarily associated with molecules unlike the bulk counterparts. The clusters are the superfine 0D particles which exhibit several peculiar physical as well as chemical properties [24,25].

Transition metal (TM) oxides are fascinating classes of materials when characteristics as well as applications are taken into account [26,27]. Because of their intriguing structural, electronic, magnetic, photonic [18], florescences [28] and biological properties as well as utilization in several energy storage and conversion applications such as super-capacitors, optoelectronics [29], lithium-ion-batteries and electrolysis, these TM oxides are of great interest [30]. The exceptional properties of said materials owe to metals-oxygen bonds which may change from ionic to highly metallic or covalent character. The nature of TM valence d-electrons is vital to describe the electronic and magnetic configuration of these materials.

The 2D TM oxides has been proved to be a better candidate for several applications specifically the surface dependent properties such as catalysis, optoelectronics [31], thermo-electronics, magneto--electronics, gas sensing and photo-catalysis due to their larger surface area as large number of atoms are readily available at surfaces [32]. Besides these, the fascinating physical characteristics as well as attractive applications in Nanoelectronics, the semiconductors based on 2D materials are of great fascination for researchers [17]. The 2D semiconductors are better candidates for channel materials because of upgraded carrier transport linked with the unavailable dangling bonds as well as decreased scattering at the smooth surfaces. In contrast to other 2D materials, 2D TM oxides exhibit distinct electronic properties, catalytic performance, thermal stability as well as mechanical strength.

The exploration of new materials is hot research topic in material science when applications are taken into account. However, in order to use them in the application, the detailed analysis of properties of the materials is required. The structural and electronic properties of new structures have been carried in order to gather the necessary information for utilization and synthesis of the material. The electronic properties extracted via density of states and band structure calculations strongly depend upon valence shell configuration and hence shed light on bonding, chemical reactivity and transport phenomenon of the material. In case of transition metal (TM) oxides, the TM atoms employ d-states while oxygen offers p-states as valence shell configuration. Hence, in majority of TMOs, the valence band (VB) is formed via O-2p states while the conduction band (CB) is formed by the TM-3d states when major contributions are taken into account. The metallic and semiconducting conductivity of the materials is decided on the basis of position of Fermi level and overlap of CB and VB. The conductivity trends in case of TMO's NiO, VO_2, NbO_2, Ta_2O_5 has been comprehensively investigated [33–37].

Tantalum, a well-known 5d transition element, is famous for the formation of various compounds having a number of applications. Tantalum and its oxides (i.e. TaO, TaO_2, TaO_3 and Ta_2O_5) have extensively been investigated for several applications such as dielectric materials for the electronic devices and state of art ballistic materials for their utilization in defense industry [38]. Tantalum shows great affinity towards oxygen and as a result forms a strong surface oxide films, which makes it a potential candidate for catalytic applications. For instance, the stable phase of tantalum oxide i.e. monoclinic Ta_2O_5 has been utilized as a catalytic material for the removal of NO_x at commercial-scale applications. Nevertheless, tantalum leads to the formation of greater than 25 metastable oxides that are, in most of the cases, in contest with the stable Ta_2O_5 specifically in thin films as incorporated by means of non-equilibrium processing approaches [39]. The metastable tantalum oxides are formed on extensive range of the content of oxygen and hence maintain a greater number of the oxidation states. This creation of metastable oxides could take place at ambient as well as elevated temperatures and also in the grain boundaries and several other regions of higher lattice strain. This is specifically of greater interest in nanocrystalline materials because of their intrinsically larger grain boundary volume fraction. In addition to all the facts, considering tendency to quickly evolve by several unstable structures prior to establishing an equilibrium states, the separation as well as the characterization of these metastable phases is very difficult.

TaO_2 is found in different structural phases especially rutile class of structure having a tetragonal configuration [40–43]. The different phases of binary structure of Ta–O compounds change as a function of temperature due to which its synthesis is difficult. These oxides have been found suitable for photo-catalytic as well as photoelectrochemical (PEC) water splitting for hydrogen generation [44,45]. It has been found that the application of these oxides strongly depends upon choice of phases, structural polytypes, dimensionality, and layeredness due to which the current state of knowledge needs updating [46]. This study is of first of its kind which reports detailed investigations on Ta oxides in 3D, 2D, 1D and OD. A brief comparison of structural and electronic properties is also given, that shed light on the effects of downscaling on the properties of tantalum oxides materials.

2. Computational details

The work reported here comprises of density functional theory (DFT) based computations of structural and electronic properties predicted by solving the Kohn-sham equations for the cubic lattice unit cell of TaO, Tetragonal unitcell of TaO_2, hexagonal structure of TaO_3 and monoclinic structure of Ta_2O_3 [47–49]. The periodicity as bulk, slab, chains, and clusters were used to investigate the 3D, 2D, 1D and 0D structures of the mentioned materials, respectively. The entire calculations were performed using DFT based ADF-BAND code which employs linear combination of atomic orbitals to study the periodic systems [50–53]. First of all, the geometries of all the structures were fully relaxed in geometry optimization runs after which computation of the electronic properties via single point calculations were carried out.

For the accuracy of the DFT calculations, two parameters are of great importance that are exchange correlation functional and basis sets. These parameters are set on the basis of materials and the dimensions of the materials and it should be noted that one parameters that is best for one material may not be suitable for other materials but for the comparison purposes similar computational details were used. The geometry of the above mentioned oxide materials were optimized at GGA-PBE level of theory which is well-known for estimation of structural trends and physical properties [54]. The Qausi-Newton method having BFGS such as Hessian update methodology was applied for the geometry optimization of periodic systems. For convergence during SCF cycles, the direct inversion of iterative subspaces (DIIS) methodology was utilized [53]. The electronic properties were calculated under single point (SP) calculations by using the GGA-PBE and TB-mBJ (Tran and Blaha modified Becke-Johnson potential) functional. The functional TB-mBJ calculates the electronic properties of the materials; specifically the metal oxides and transition metal oxides close to the experimental values and provides the significantly better description of electronic properties to provide valuable predictions [55–57]. The trend obtained in both of the cases (GGA-PBE & TB-mBJ) is similar though a minor impact on the values is observed. The DFT code uses basis functions having slater-type orbitals (STOs) that are well-known to estimate the behavior closer to the nucleus. For geometry optimization and for the single point calculations of bulk tantalum oxides, the triple zeta polarization (TZP) basis was used. In TZP, the TZ represent the atomic orbitals i.e. s, p etc. whereas "P" denotes the polarization factor and the angular momenta terms. The TZP basis set, includes a function having two greater moments as compared to the required by the occupied atomic orbitals. As the electronic configuration of Tantalum (Ta) is [Xe] $4f^{14}$, $5d^3$, $6s^2$ so the frozen-core approximation "large" was used which would freeze/isolate the core electrons and hence speed-up the calculations. In

ADF, the numerical quality is determined by k-point grid, density fitting and basis sets. For structural properties (geometry optimization) the numerical quality (normal) was used while for the single point calculations, numerical quality 'good' was taken into account. In these calculations, the scalar relativistic effects were taken into account whereas few calculations were carried out to check the effects of spin-orbit coupling (SOC). For instance, the formation energy of 2D TaO_2 with the GGA-PBE functional, scalar relativistic effect and TZP basis sets was −2.63 eV/atom which was lowered to −2.69 eV/atom when SOC was included. Therefore, owing to weak effects, the SOC were not considered. The energy convergence, gradient convergence and step convergence were taken as 10^{-6}, 10^{-3}, 10^{-3} eV/atom respectively for all calculations. The size of the clusters are computed by using the formula given in equation (1) [53,58].

$$d = \left(\frac{3a^2c(2n_{Ta} + n_o)}{4\pi} \right)^{1/3} \quad (1)$$

Where 'd' represents the effective size of the clusters, 'a' and 'c' are the optimized lattice constants and n_{Ta} and n_O are respectively the number of atoms of Ta and O in the structure of clusters.

The formation energy was computed using relation $E_F = E_{Products} - E_{Reactant}$ by equalizing the number of atoms in the reactants and products. For example, the formation energy for TaO_3 was computed by $E_f = E(Ta_2O_6) - 2E(Ta) - 3E(O_2)$. The trimming of the 3D bulk material was carried out by introducing a missing axis along z-axis to produce 2D slab in xy-plan, two missing axes along x- and y-axis to produce 1D chain along z-axis and three missing axes to produce 0D clusters. The GUI "Graphical User Interface" in ADF-BAND ensures sufficient vacuum along the missing axis of zero, one and two dimensional materials.

2.1. Description of crystallographic information files (CIF)

In case of TaO, the unit cell formula is TaO, consists of 2 atoms, in which one is Ta and other is O as given in Fig. 1 (a). The lattice parameters were a = 3.18713 Å, b = 3.18713 Å, c = 3.18713 Å where the angles were $\alpha = 60^0, \beta = 60^0, \gamma = 60^0$. The crystal system was cubic with point group m3m. The volume of the unit cell was 22.8919 Å^3. The size of super cell was 2 × 2 × 2 having (16 atoms) for bulk and 2× 2 having (8 atoms) for the slab. The unit cell formula of TaO_2 was Ta_2O_4 (having two formula units) consisting of two atoms of Ta and 4 oxygen atoms, and hence total 6 atoms in a unitcell as shown in Fig. 1 (b). The lattice parameters were a = 5.00715 Å, b = 5.00715 Å and c = 2.87610 Å while angles were $\alpha = 90^0, \beta = 90^0, \gamma = 90^0$. The crystal system was tetragonal having point group 4/mmm and space group number 136. The volume of unit-cell was 72.1082 Å^3. The size of super cell in bulk was 2 × 2 × 2 (48 atoms) and for slab, the size of super cell was 2 × 2 (24 atoms). The unit cell of TaO_3, as given in Fig. 1 (c), contains 2 Ta atoms and 6 O atoms and hence the unit cell formula was Ta_2O_6. The total number of atoms in a unit cell were 8. The crystal structure was hexagonal having space group p63/mmc and space group number 194. The lattice parameters per CIF were a = 4.67565 Å, b = 4.67675 Å and c = 3.72424 Å where the angles in degree are as $\alpha = 90, \beta = 90, \gamma = 120$ and unit cell volume was 70.510057 Å^3. The respective size of super cell for bulk and slab were 2 × 2 × 2 and 2 × 2. The unit cell formula for Ta_2O_3 was Ta_4O_6 which comprises of 4 Ta atoms and 6 O atoms as given in Fig. 1 (d). The lattice parameters (as per CIF) were a = 11.92147 Å, b = 2.83789 Å and c = 7.59566 Å. The angles were $\alpha = 90^0, \beta = 113.83^0, \gamma = 90^0$. The crystal system was monoclinic having space group $C2/m$ and space group number 12. The unit cell volume was 235.062 Å^3. The size of super cell in bulk was 2 × 2 × 2 (80 atoms) and for slab, the size of super cell was 2 × 2 (40 atoms).

3. Results and discussion

In this section, the calculated results on structural and electronic properties of the mentioned materials are described. For structural properties, bond lengths, bond angles, formation energy, charge analysis, size of clusters and bonding were taken into account, while the electronic properties are discussed on the basis of density of states (partial and total) and band structure.

3.1. Structural properties

The calculated structural parameters including bond length, bond angles along with charge analyses are described in detail. The optimized structures of the said materials are given in Fig. 2 whereas the values of bond lengths of the entire materials studied herein are given in Table. 1. The results reveal that bond length and bond angles decrease in most of the cases as we move from the bulk to the lower dimensions which agrees with the relevant literature. However, in case of the TaO_2, the clusters show deviations. The abnormal behavior in the said materials may be attributed to the effect of computational details specially for the functional. The size of the clusters found using equation (1) computed

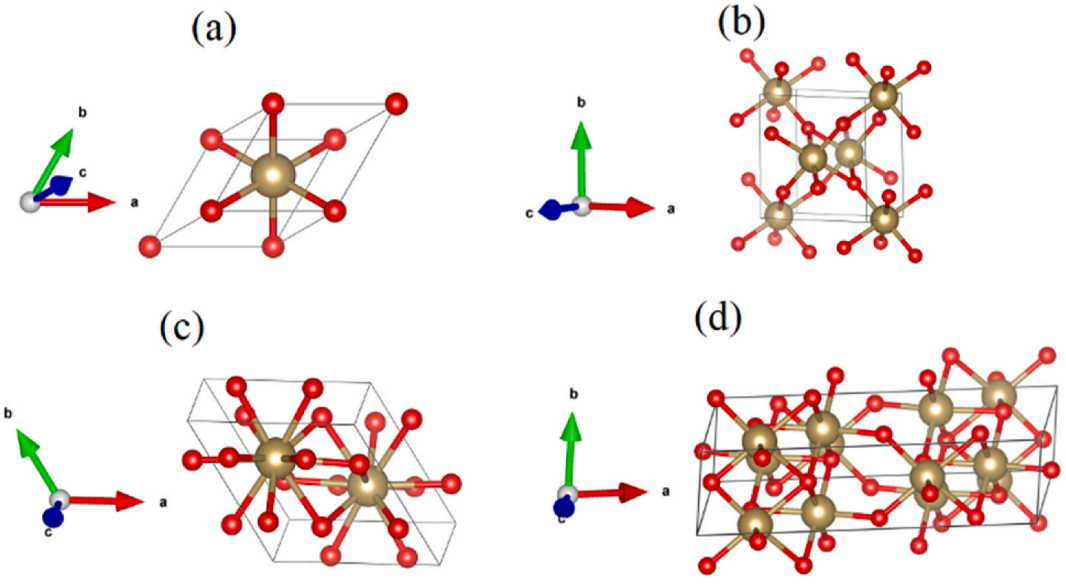

Figure-1. The crystal structure in bulk for (a) ***TaO*** (b) ***TaO***$_2$ (c) ***TaO***$_3$ (d) ***Ta***$_2$***O***$_3$ where red balls represents the O atoms and others represent the Ta atoms.

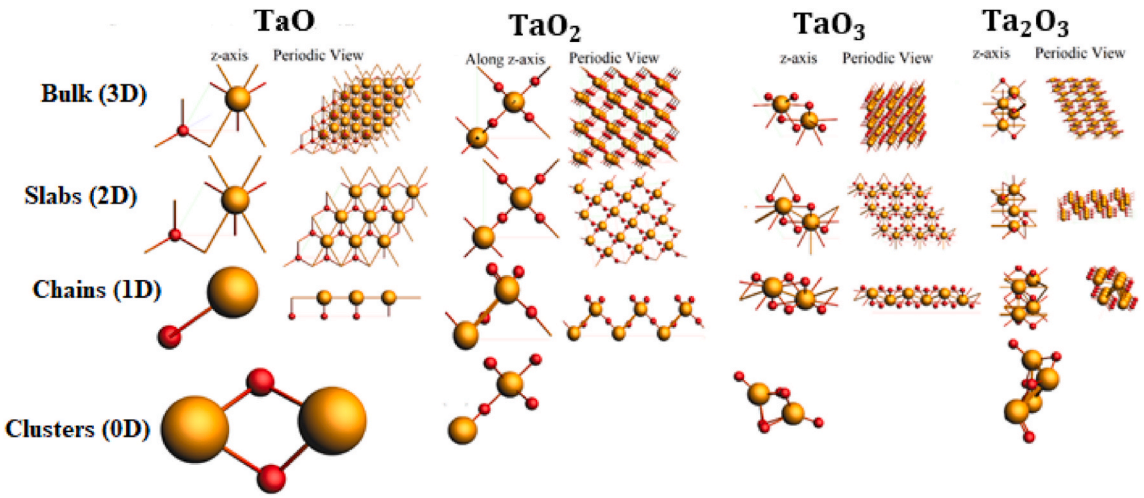

Figure-2. The optimized structure along z-axis and periodic view of TaO, $\mathbf{TaO_2}$, $\mathbf{TaO_3}$ and $\mathbf{Ta_2O_3}$ in form of bulk, slab, chains and clusters. Orange and red colored spheres represent Ta and O atoms respectively.

Table-1
The optimized bond lengths in angstroms b/w Ta–O of *TaO*, TaO_2, TaO_3 and Ta_2O_3 in bulk, slab, chains and clusters periodicities.

	TaO	TaO_2	TaO_3	Ta_2O_3
Bulk	3.90	2.05	2.24	2.29
Slab	2.09	1.91	2.03	2.16
Chains	1.74	1.79	1.96	2.13
Clusters	1.7	2.09	1.74	1.74

for *TaO*, TaO_2, TaO_3 and Ta_2O_3 are 0.28 nm, 0.409 nm, 0.37 nm, and 0.49 nm respectively.

In general, Ta being transition metal exhibits the electropositive nature, while the oxygen exhibits the electronegative nature. The Hirshfeld charge analysis was carried out to understand the transfer of charge inside the materials and the computed values are in theTable. 2 which shows that the charge is transferred from Ta atoms to the oxygen atoms. By observing the charge on individual atom, it was found that for bulk and slab periodicity, the amount of charge on every Ta and O atom is same, while for chains and cluster, the charge on different Ta atoms is different. Similar trend is observed in case of O atoms where charge on every O atom is different. In general, for slabs, chains and clusters, every Ta and O should represent distinct behavior and the differences are due to the breaking of periodicity and appearance of the dangling bonds. The slab is not showing this behavior because it is very thin. However, if the slab thickness is increased then it may exhibit behavior similar to the chains and clusters.

The dipole moment is computed along the missing axis so it is represented by all the periodicities except the bulk (3D) due to the presence of periodicities along each axis. The dipole moment calculated for 2D TaO is −0.0087 Debye (along z-axis). While the dipole moment for chains are 2.0839 Debye and 1.4735 Debye along y- and z-axis. The dipole moment computed for TaO_2 unitcell in slab periodicity is 0.0000 Debye.

In order to estimate the bonding between the Ta and O atoms, the electronegativity difference is an important parameter whose value is 1.94 as per Pauling scaling, which indicates that the bonding between the Ta and O contains more than 50% ionic character. The analysis of computed formation energy is made to know least energy configuration in search of the stable structures. The value of formation energy for all the said materials as given in the Table. 3 was computed by using the formula $E_F = E_{Products} - E_{Reactants}$. For example, for TaO_3 having the unit cell formula Ta_3O_6, the formation energy was computed using $E_F = E_{Ta_2O_6} - 2E_{Ta} - 3E_{O_2}$.

The majority of the materials appeared to have the negative formation energy pointing to exothermic reactions and hence likelihood of their experimental growth. In case of *TaO* only bulk and slabs are feasible whereas the rest of the materials exhibited endothermic reactions. The bulk of the material appeared as most stable configuration whereas a small difference between the formation energies of bulk and slab is found which points to probability of transformation of the bulk to the slab. The formation energy for the slab in super cell with size 2×2 is −1.10 eV/atom whereas its value for super cell with size $2 \times 2 \times 2$ is −1.62 eV/atom. In case of TaO_2, the formation energy for bulk is minimum and for clusters it is maximum which indicates decrease in its stability when dimensions of TaO_2 increases. Since, the energy is minimum for bulk TaO_2 as compared to other dimensions, hence the material will be most stable in bulk. The difference of formation energy in bulk

Table-3
The formation energy per atom (eV/atom) of the materials under study in all 4 periodicities.

	TaO	TaO_2	TaO_3	Ta_2O_3
Bulk	−1.56	−3.08	−1.90	−2.73
Slab	−1.16	−2.63	−1.60	−2.35
Chains	0.25	−2.02	−1.67	−2.61
Clusters	1.05	−1.88	−2.01	−1.99

Table-2
The Hirshfeld charges (in units 'e') of *TaO*, TaO_2, TaO_3 and Ta_2O_3 in bulk, slab, chains and clusters periodicities.

	TaO		TaO_2		TaO_3		Ta_2O_3	
	Ta	O	Ta	O	Ta	O	Ta	O
Bulk	0.226	−0.266	1.11	−1.11	1.224	−1.224	1.452	- 1.454
Slab	0.211	−0.21 1	1.29	−1.288	1.398	−1.398	1.562	−1.562
Chains	0.242	−0.242	1.211	−1.211	1.5	−1.495	1.604	−1.604
Clusters	0.287	−0.287	1.338	−1.339	1.63	−1.629	2.047	−2.047

and slab is less as compared to the bulk and clusters so TaO_2 can be converted into slab/surfaces upon exfoliation processes with low probability of agglomeration. Similarly, the value of formation energy for the super-cell in bulk and slab having respective sizes 2× 2× 2 and 2× 2 was −3.18 eV/atom and −2.63 eV/atom respectively. The formation energy computed for the clusters of 48 atoms was −2.85 eV/atom. In super cell of bulk and clusters, the number of atoms is same, but the energy of bulk is notably low which indicates low probability for this material to be agglomerated.

The energy profiling of Ta_2O_3 in different periodicities indicates the stability order will be Clusters > bulk > chains > slabs. It means this material has a greater probability to exist as clusters as compared to the bulk. There is least probability for this material to exist in form of 2D slabs. The formation energy of super cell in bulk and slab having size of $2 \times 2 \times 2$ and 2×2 is about −1.87 eV/atom and −1.54 eV/atom for same number of atoms in the structures respectively. For Ta_2O_3 the stability order is found as bulk > chains > slabs > clusters which means that there is an easy transformation from bulk to chains as the minor energy difference as compared to others. There is least probability of agglomeration upon synthesis of this material. The formation energy for bulk and slab super cell having size of $2 \times 2 \times 2$ and 2× 2 was −2.88 eV/atom and −2.75 eV/atom respectively.

3.2. Electronic properties

This section sheds light on the electronic properties based on the density of states (DOS) and band structures. For all cases, the total DOS are represented by the black color, while the contribution of Ta and O atoms are represented by red and blue colors respectively.

3.2.1. TaO

The total density of states (TDOS) for bulk, slab, chains and clusters *TaO* are shown in Fig. 3. The partial DOS represents the contribution at Fermi level and in regions of bands close to the Fermi level. The partial DOS for bulk *TaO* are given in Fig. 3 (i) which indicates that the material shows the metallic behavior in bulk as the states pass through the Fermi level. At Fermi level, the major contribution is from the d-orbital of Ta-atom while p-orbital of oxygen atoms shows a minor contribution. The contribution of oxygen (at ∼ −5 eV) far from Fermi level is observed.

Since the d-orbital shows the major contributions at the Fermi level as per d-orbitals of Ta plotted in Fig. 3 (i). By observing the pDOS, it is clear that almost all the orbitals have an equal contribution. The p-orbital from O atom offers very minor contribution as compared to the d-orbital of Ta at Fermi level. By considering the pDOS of 2D TaO, the Ta-d shows the major contribution at Fermi level and at ∼1 eV. The DOS plotted in Fig. 3 (ii) reveal that the slabs exhibit metallic behavior. Almost the entire d-orbitals have an equal contribution as given Fig. 3 (ii). In bands at and above the Fermi level, the major contribution are found dominated by 5d-z^2. The minor contribution is from p-orbitals of O whereas $2p_y$, $2p_z$ have almost an equal contribution. The pDOS of 1D (chains) *TaO* is depicted in Fig. 3 (iii) which reveal that the major contribution at Fermi level and above arises from Ta-atom. The contribution of oxygen is negligible at Fermi level and at ∼ −4 to −5 eV whereas minor contribution of oxygen is observed. The d-states of the Ta has maximum contribution at Fermi level and almost all the orbitals have same contribution. The clusters exhibited metallic behavior due to contribution of d-orbitals of Ta atoms at Fermi level as shown in Fig. 3 (iv). So, it can be concluded that the bulk, slab, chains and clusters show metallic character due to the presence of states from Ta at Fermi level. The sharpness of peaks is found reduced on moving to low dimensions due to confinement of electrons.

The band structure gives a more detailed description of electronic properties by giving the interaction of s, p, d and f orbitals. Here, the band structure of 3D and 2D *TaO* are given. For the supercell of *TaO*, the band structure at high symmetry points is presented in Fig. 4 where d-states and p-states are indicated by arrow heads. The material possesses

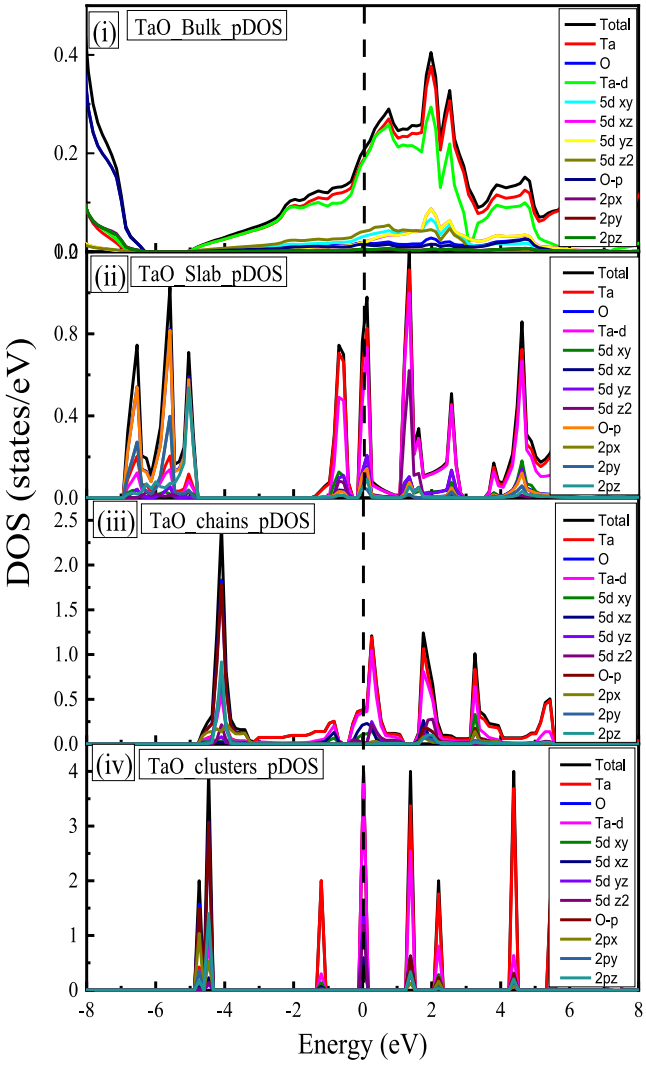

Figure-3. The total and partial Density of states of ***TaO***, Where (i), (ii), (iii) & (iv) represent bulk, slab, chains and cluster periodicities respectively.

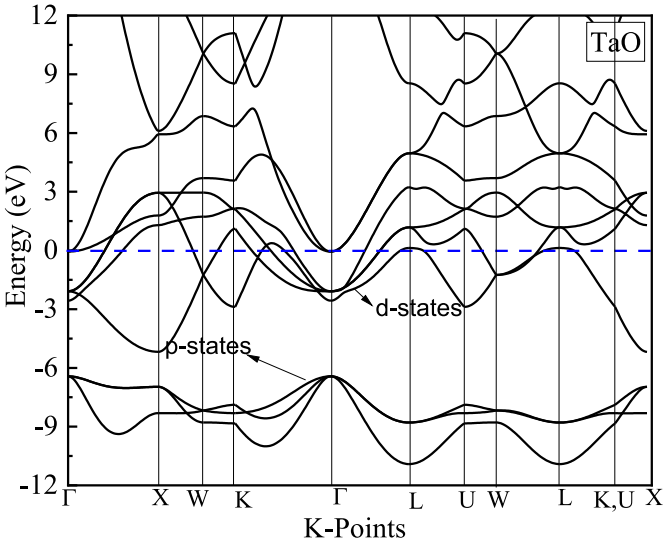

Figure-4. The calculated band structure for 3D-TaO.

the metallic behavior. In case of the unit cell of the slab, the band structure along the high symmetry points γ, M, K is shown in Fig. 5. Furthermore, the results reveal that the 2D-*TaO* exhibits the metallic nature as Fermi level passes through Ta-d states as well as p-d hybrid states. In the band below the Fermi level, hybridization of the s and d orbital is observed while in deeper bands from −3.5 eV to onward, a major contribution of the p-orbital is observed.

In the band close to Fermi level, there is the major contribution of d-orbitals whereas in the above bands s-d hybridization and somehow s-p-d hybridization is observed. In case of chains, the computed band structure indicates the major contribution of d-orbital at Fermi level and closer bands. In the region above Fermi level, there is the p-d hybridization whereas at further high energies s-p hybridization is noticed.

3.2.2. TaO_2

The total and partial DOS for TaO_2 in form of bulk, slab, chains and clusters are shown in Fig. 6. It seems that as the dimension decreases (from bulk towards clusters), the number of peaks in DOS increases and become sharper. In case of bulk, the atoms are surrounded by the other atoms in three dimensions and interact in all dimensions due to which their DOS appearing in the form of band as can be seen in this case for bulk TaO_2. The number of surrounding atoms decrease as the dimension of the material decreases. Hence the levels are not properly split as for that of the bulk and appear as atomic level rather than a band. This is the reason that the peaks of TaO_2 clusters are sharper in comparison to the bulk, slab or chains. In case of bulk, slab and clusters, the material shows the metallic behavior as the states Ta and O atoms are found at Fermi level, while in chains, the material behave as semi-conductor having band gap of about 0.2–0.3 eV.

The change in dimensions of the materials from bulk to chains pointed to a transition from metallic to semiconducting nature as per quantum confinement effect.

The pDOS of TaO_2 in bulk is depicted in Fig. 6(i) which reveals metallic behavior due to the major contribution of Ta-d states at Fermi level where contribution of 5d-z^2 is maximum, while a minor contribution of 5d-xy is also present. The pDOS of TaO_2 in slab periodicity are shown in Fig. 6 (ii) that reveals that at Fermi level and at up to – 0.5 eV (i.e. region very close to the Fermi level), the Ta-d-orbital (specifically the $5d_{z2}$) has major impact. The bands in region deep below the Fermi level (i.e. −4.1 eV to downwards) is formed by the $2p_y$ and $2p_z$ states of oxygen.

The chains of TaO_2 exhibits semiconducting behavior with band gap of about 0.2–0.3 eV, having the major contribution from the d-orbitals of

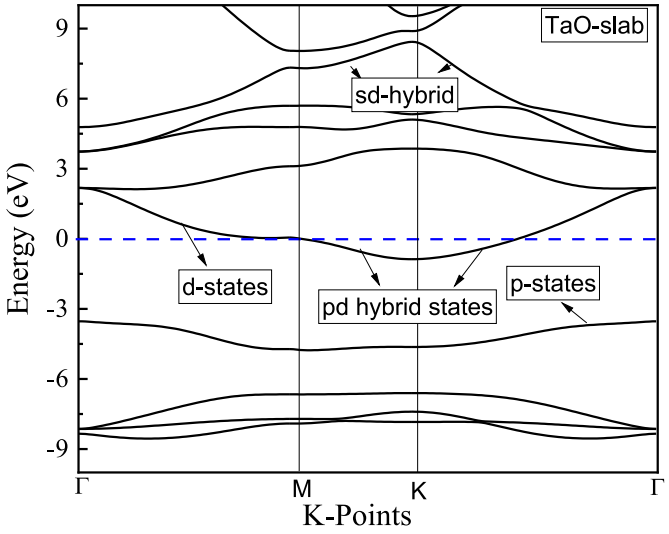

Figure-5. The band structure as computed by TB-mBJ for the 2D-TaO. Where the Fermi level is shifted to 0 eV.

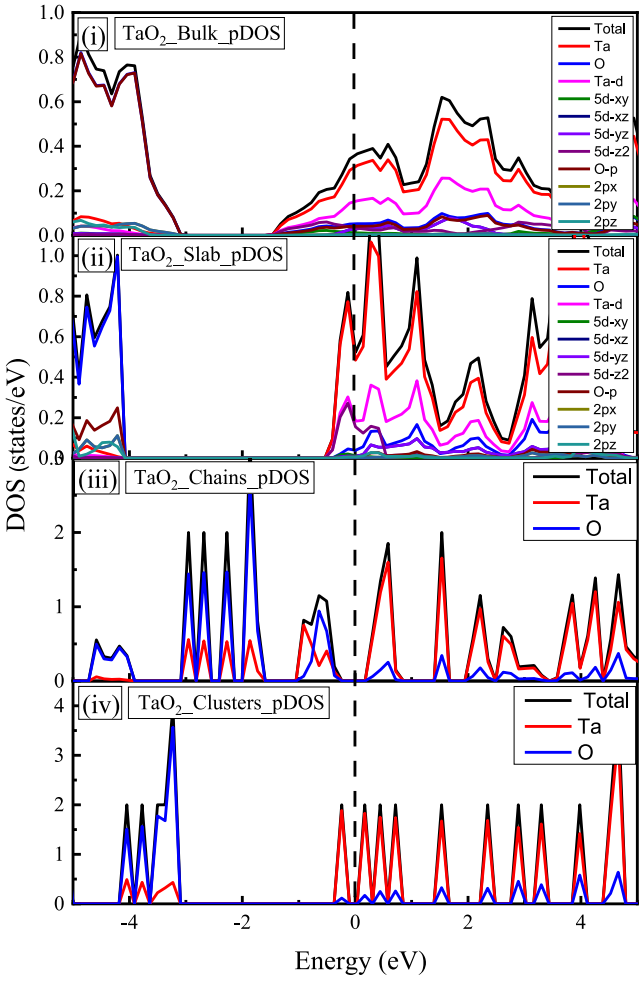

Figure-6. The total and partial Density of states of TaO_2, Where (i), (ii), (iii) & (iv) represent bulk, slab, chains and cluster periodicities respectively.

Ta in CBM (Conduction band minima) and the p-orbitals from O in VBM (valence band maxima) as depicted in Fig. 6 (iii). The 0D material of TaO_2 i.e. in the form of cluster is a narrow band gap semiconductor with the band gap of ~0.1 eV, having the major contribution from Ta in CBM and O in VBM as shown in Fig. 6 (iv).

The band structures of TaO_2 for bulk, slab and chain periodicities were computed and the band structure for the bulk periodicity is shown in Fig. 7, which reveals the metallic behavior due to the presence of d-orbitals at Fermi level. The slab model of the material shows the metallic behavior due to d-states of Ta-atoms at Fermi level.

3.2.3. TaO_3

The total DOS and partial DOS showing contribution of Ta as well as O atoms for TaO_3 are drawn in Fig. 8 (i) which reveals that bulk TaO_3 offers a metallic character as the O-p states are found at Fermi level. Similarly, the states at ~1.5 eV reveal major contribution from Ta atoms and minor contribution of O atoms. In the region close to the Fermi level the major contribution from $5d_{xy}$ is noticed whereas in regions above Fermi level the contribution from $5d_{yz}$ and $5d_{z2}$ is observed.

The major contribution in region close to the Fermi level arises from O-2p [45]. Fig. 8 (ii) reveals that the slab periodicity of TaO_3 exhibits the metallic nature due to major contribution from Ta-d orbitals at Fermi level. The contribution from 5d-z^2 is maximum in region above Fermi level as shown in Fig. 8 (ii). The contribution of oxygen p-orbitals with major part of $2p_x$ and moderate role of $2p_y$ and $2p_z$ is observed below Fermi level. The 1D of TaO_3 offers the metallic behavior as the states

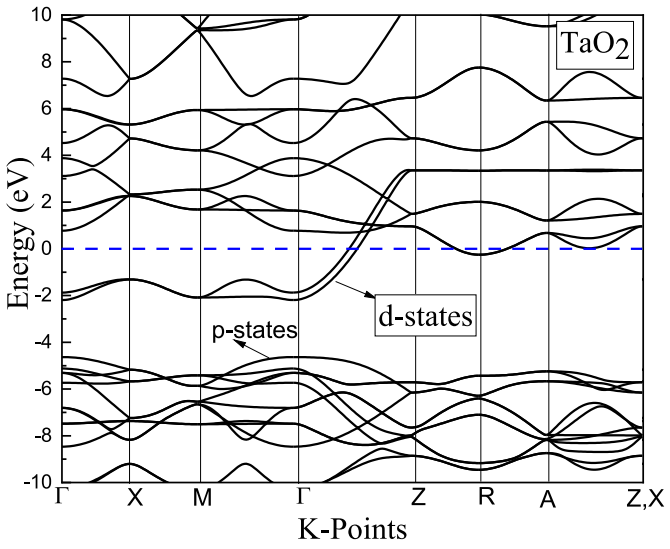

Figure-7. The computed band diagram of TaO_2 in bulk periodicity. The Fermi level is shifted to 0 eV.

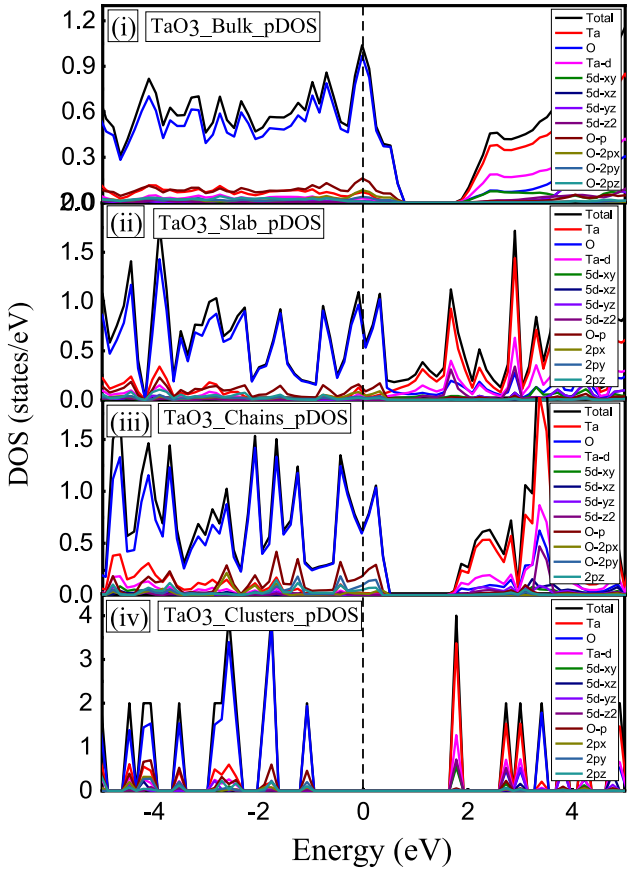

Figure-8. The total and partial Density of states of TaO_3, Where (i), (ii), (iii) & (iv) represents the respective DOS in bulk, slab, chains and cluster periodicities respectively.

passes through the Fermi level as shown in Fig. 8 (iii). The pDOS reveals that at Fermi level the major contribution arises from p-orbitals of O atoms and d-orbitals of Ta atoms. In region above Fermi level, the major contribution arises from Ta 5d-z^2, while the states below Fermi level comprise of almost equal contribution of O-p orbitals. At Fermi level, the minor contribution arises from the states 5d-z^2 and major contribution arises from the states $2p_y$, $2p_z$ and $2p_x$ respectively. The sharpness of peaks is due to the quantum confinement as for chains the atoms are present in the line and hence the interaction is only along the 1D that results in the sharpness of peaks rather than the formation of bands. The clusters are semiconductor having band gap of about 2.6 eV. The d-orbitals contributes from Ta atoms and hence major contribution in CB is from 5d-z^2 as shown in Fig. 8 (iv). Similarly, the VB is formed by major contribution of $2p_y$ and minor contribution of $2p_z$. In all cases of TaO_3, the band above Fermi level is mainly formed by Ta states whereas the bands below Fermi level got major contribution of O states. The results are in good agreement with the understanding that as the dimension decreases a transition from metallic to semiconducting character takes place due to quantum confinement.

The band structure of TaO_3, as computed for bulk, slab and chains and the band structure for bulk periodicity of said material is represented in Fig. 9. The results showed that the Fermi level is covered with p-states which points to the metallic character. In bulk TaO_3, there is no s-d hybridization in region above Fermi level in contrast to the slab and chains. The bands below the Fermi level are formed by O-p orbitals. The slab and chain periodicities TaO_3 shows the metallic behavior.

3.2.4. Ta_2O_3

The total and partial DOS of bulk Ta_2O_3 are given in Fig. 10 (i), that reveals the bulk Ta_2O_3 is metallic as the states passes through the Fermi level. In region above the Fermi level, the Ta-d orbitals contribute mainly while O-p orbitals offer a minor contribution as shown in Fig. 10 (i). Though Ta-d orbitals contribute but major contribution of O-p orbitals is noticed in the region below the Fermi level.

The total and partial DOS of Ta_2O_3 in slab periodicity are given in Fig. 10 (ii) which reveals metallic character similar to the bulk Ta_2O_3. The region above Fermi level is formed by Ta-d states with small contribution from s and p-orbitals of oxygen as shown in Fig. 10 (ii). At Fermi level the maximum contribution arises from the $5d_{xz}$ orbitals, while the $5d_{yz}$ also offers a considerable contribution above Fermi level. On the other hand, in case of the bands located below Fermi level, the $2p_z$ offers the maximum contribution with moderate role of $2p_x$ and $2p_y$ states. The 1D material of Ta_2O_3 also appeared metallic due to presence of Ta-d and O-p states at Fermi level as shown in Fig. 10 (iii). The 0D material of Ta_2O_3 in the form of clusters appeared a narrow gap semiconductor with band gap of about 0.2 eV, having the major contribution from Ta-d states in CB and O-p states in VB as shown in Fig. 10 (iv). The bulk and slab periodicity of Ta_2O_3 possess metallic behavior as per band

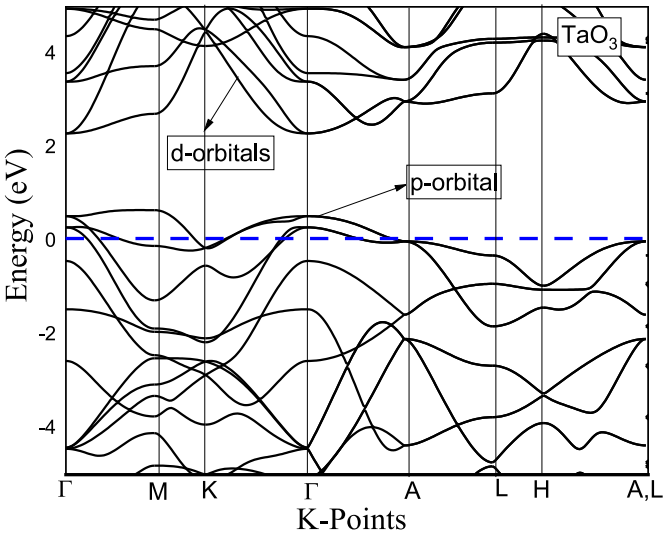

Figure-9. The computed Band structure as calculated by TB-mBJ in 3D for TaO_3. Where the Fermi level is shifted to 0 eV.

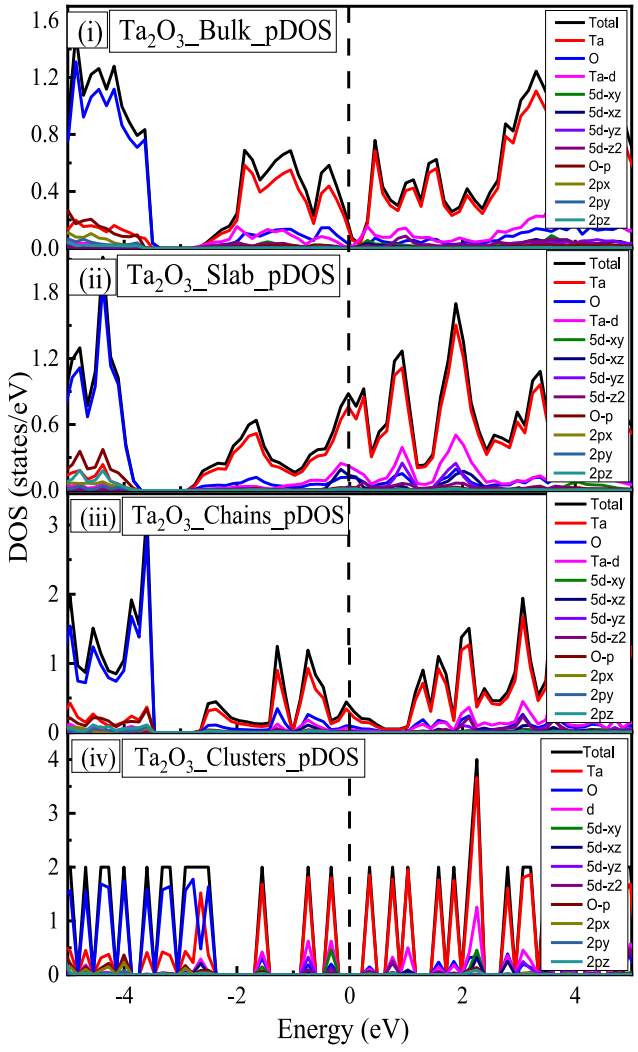

Figure-10. The total and partial Density of states of Ta_2O_3, Where (i), (ii), (iii) & (iv) represent bulk, slab, chains and cluster periodicities respectively.

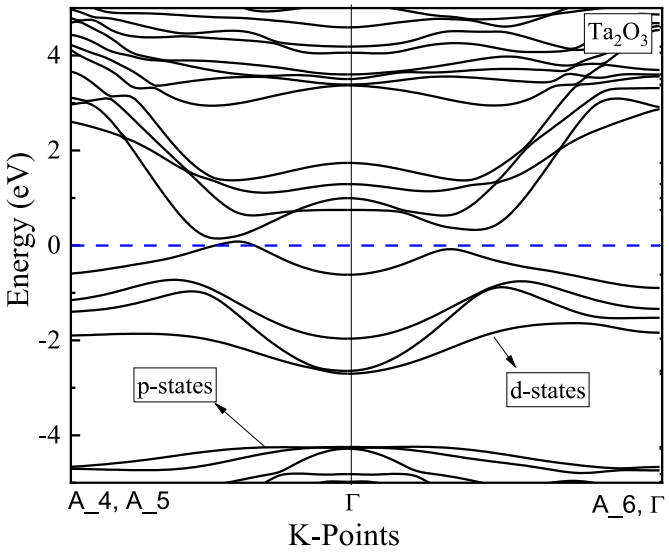

Figure-11. The computed Band structure in 3D for Ta_2O_3. The Fermi level is shifted to 0 eV.

structure of the bulk periodicity shown in Fig. 11.

4. Comparison with experimental results

The reported literature is deficient on experimental synthesis of tantalum oxides. TaO_2 is one of the metastable compound in the Ta–O binary systems whose synthesis in single phase is challenging [43]. The TaO_2 exists in several polymorphs but in majority of cases rutile phases in tetragonal structure has been obtained due to which this structure was taken in the current study. The synthesized *TaO* has been found stable in cubic structure which was taken as starting material in this study. The experimentally reported value of bond length in case of bulk TaO_2 is 1.99 Å which is close of the value obtained in this work i.e. 2.05 Å [59]. Similarly, the bond length Ta–O in nanowires (1D) of TaO_2 is 2.06–1.85 Å, while the bond length obtained in current study is about 2.05–1.79 Å which shows close agreement. The difference in the bond lengths may be attributed to the well-known underestimation of the lattice constants of the GGA-PBE functional and impact of the relativistic effects on Ta atoms [60]. The bond length Ta–O in structures related to TaO_2 (i.e. TaON) ranges from the 2.03–2.15 Å [61] which is in great agreement with obtained in this work. Similarly, the lattice parameter as computed by GGA-PBE for the materials are a = 4.97 Å, b = 5.03 Å, c = 5.18 Å, α = 90, β = 99.7, γ = 90, while the experimental values are a = 4.97 Å, b = 5.04 Å, c = 5.18 Å, α = 90, β = 90, γ = 90[59–61]. In a similar case of $SmTaO_4$, the PBE calculated values of bond lengths are 1.986 Å, 2.04 Å which are in agreement with the experimental values 1.84 Å, 1.92 Å, and 2.335 Å [62]. Likewise, the lattice parameters are also compared whereas the difference of 1.16% is observed. Moreover, the PBE calculated value of band gap is 3.49 eV while the experimentally obtained band gap was 3.68 eV. The analysis of calculated electronic properties reveals that *TaO* is metallic which also agrees with the experimental literature [63].

5. Summary

The computations on Ta oxides in all possible periodicities were carried out. The findings pointed out decrease in bond lengths and bond angles whereas increase in band gap when Ta oxides are downscaled from bulk to clusters although, for the TaO_2 the abnormalities in structural and electronic properties are observed. The peaks in DOS becomes sharp with decrease in dimensionality of the studied materials which points to localization and confinement of the electrons.

The formation energy of bulk *TaO* is least as compared to the slab, chains and clusters which indicates the stabilization of the material in bulk. There is minor energy difference of the formation energy between the bulk and slab, but the difference between the bulk and chains/clusters is very large. This means that there is a possibility to grow *TaO* in 2D surfaces but there is low likelihood for accumulation or aggregation in the form of clusters. The *TaO* in all periodicities has metallic character due to the presence of d-electrons at fermi level and the overlap of conduction and valence band.

In case of TaO_2, as we move towards lower dimensions, a decrease in bond length and bond angles is noticed. The electronic properties reveals that the bulk, slab and clusters of TaO_2 are metallic in nature due to presence of d-states of Ta, while the chains appeared semi-conductor having the band-gap of about 0.2–0.3 eV. It means as the dimension decreases, a transition from metallic to semiconducting character is observed except for the clusters which appeared to deviate from the trend.

The formation energy of TaO_3 per atom are −1.90 eV/atom, −1.60 eV/atom, −1.67 eV/atom and −2.01 eV/atom for bulk, slab, chains and clusters respectively. It reveals that clusters are of greater stability as compared to bulk whereas slab was considered as the least stable. The electronic properties reveal that bulk, slab and chains are metallic because of major contribution of p-states of O-atoms at Fermi level while the clusters are semiconductor having band gap of about 2.6 eV.

The formation energy analyses of Ta_2O_3 reveals the stability of the material in bulk as compared to the other periodicities. The energy difference between the bulk and chains are less as compared to the difference between bulk and slabs/clusters which means that formation of chains is more feasible as compared to the slabs or clusters. The electronic properties reveals that all the periodicities i.e. bulk, slab and chains are metallic because of d-states and again the clusters appeared semiconductors with a very narrow band gap.

Funding

This research is supported by ASPIRE, the technology program management pillar of Abu Dhabi's Advanced Technology Research Council (ATRC), via the ASPIRE Award for Research Excellence initiative.

Code availability

The code used in this study is commercially available.

CRediT authorship contribution statement

Alia Jabeen: Writing – original draft, Methodology, Investigation, Data curation. **Mohammad Alkhedher:** Writing – review & editing, Visualization, Validation. **Abdul Majid:** Writing – review & editing, Supervision, Resources, Methodology, Investigation, Conceptualization. **Najam Al Hassan:** Writing – review & editing, Visualization, Validation.

Declaration of competing interest

The authors declare that they have no known competing financial interests or personal relationships that could have appeared to influence the work reported in this paper.

Data availability

Data will be made available on request.

References

[1] A. Majid, M. Bibi, Cadmium Based II-VI Semiconducting Nanomaterials, Springer, 2018.
[2] M. Roco, Nanoparticles and nanotechnology research, J. Nanoparticle Res. 1 (1999) 1.
[3] M.A. Khalily, et al., Facile synthesis of three-dimensional Pt-TiO2 nano-networks: a highly active catalyst for the hydrolytic dehydrogenation of ammonia–borane, Angew. Chem. 128 (2016) 12445–12449.
[4] X. Xu, C. Zhang, A. Khan, T.A. Sebaey, M. Alkhedher, Free vibrations of rotating CNTRC beams in thermal environment, Case Stud. Therm. Eng. 28 (2021), 101355.
[5] M. Alkhedher, Hygrothermal environment effect on the critical buckling load of FGP microbeams with initial curvature integrated by CNT-reinforced skins considering the influence of thickness stretching, Nanotechnol. Rev. 10 (2021) 1140–1156.
[6] A. Shakoor, H. Anwar, T.Z. Rizvi, Preparation, characterization and conductivity study of polypyrrole-pillared clay nanocomposites, J. Compos. Mater. 42 (2008) 2101–2109.
[7] M. Fox, American Association of Physics Teachers, 2002.
[8] P. Tao, et al., Recent advances in exfoliation techniques of layered and non-layered materials for energy conversion and storage, J. Mater. Chem. 7 (2019) 23512–23536.
[9] Q. Wang, et al., Van der Waals epitaxial ultrathin two-dimensional nonlayered semiconductor for highly efficient flexible optoelectronic devices, Nano Lett. 15 (2015) 1183–1189.
[10] Z. Zheng, J. Yao, J. Li, G. Yang, Non-layered 2D materials toward advanced photoelectric devices: progress and prospects, Mater. Horiz. 7 (2020) 2185–2207.
[11] M. Xu, T. Liang, M. Shi, H. Chen, Graphene-like two-dimensional materials, Chem. Rev. 113 (2013) 3766–3798.
[12] X. Liu, T. Ma, N. Pinna, J. Zhang, Two-dimensional nanostructured materials for gas sensing, Adv. Funct. Mater. 27 (2017), 1702168.
[13] G. Centi, S. Perathoner, Catalysis by layered materials: a review, Microporous Mesoporous Mater. 107 (2008) 3–15.
[14] A.K. Singh, K. Mathew, H.L. Zhuang, R.G. Hennig, Computational screening of 2D materials for photocatalysis, J. Phys. Chem. Lett. 6 (2015) 1087–1098.
[15] B. Luo, G. Liu, L. Wang, Recent advances in 2D materials for photocatalysis, Nanoscale 8 (2016) 6904–6920.
[16] P.K. Kannan, D.J. Late, H. Morgan, C.S. Rout, Recent developments in 2D layered inorganic nanomaterials for sensing, Nanoscale 7 (2015) 13293–13312.
[17] Y. Pan, et al., Ohmic contacts of monolayer Tl 2 O field-effect transistors, J. Mater. Sci. 55 (2020) 11439–11450.
[18] A. Shakoor, T. Rizvi, M. Sulaiman, M. Nasir, M. Ishtiaq, Electronic properties of polyaniline doped with dodecylbenzenesulphonic acid (PANI-DBSA) and poly (methyl methacrylate)(PMMA) blends in the presence of hydroquinone, J. Mater. Sci. Mater. Electron. 21 (2010) 603–607.
[19] Y.-F. Sun, et al., Metal oxide nanostructures and their gas sensing properties: a review, Sensors 12 (2012) 2610–2631.
[20] M.I.B. Utama, X. Lu, Y. Yuan, Q. Xiong, Detrimental influence of catalyst seeding on the device properties of CVD-grown 2D layered materials: a case study on MoSe2, Appl. Phys. Lett. 105 (2014), 253102.
[21] A. Shashurin, M. Keidar, Synthesis of 2D materials in arc plasmas, J. Phys. Appl. Phys. 48 (2015), 314007.
[22] A.P. Alivisatos, Perspectives on the physical chemistry of semiconductor nanocrystals, J. Phys. Chem. 100 (1996) 13226–13239.
[23] A.A. Fedorets, E. Bormashenko, L.A. Dombrovsky, M. Nosonovsky, Symmetry of small clusters of levitating water droplets, Phys. Chem. Chem. Phys. 22 (2020) 12239–12244.
[24] M.L. Cohen, W.D. Knight, The physics of metal clusters, Phys. Today 43 (1990) 42–50.
[25] A. Majid, A. Jabeen, S.U.-D. Khan, S. Haider, Optical properties of titania–zirconia clusters: a TD-DFT study, J. Cluster Sci. 30 (2019) 707–713.
[26] J. Gopalakrishnan, S. Pandey, K.K. Rangan, Convenient route for the synthesis of transition-metal pnictides by direct reduction of phosphate, arsenate, and antimonate precursors, Chem. Mater. 9 (1997) 2113–2116.
[27] H.H. Khalid, S. Erkan, N. Bulut, Halogens effect on spectroscopy, anticancer and molecular docking studies for platinum complexes, Optik (2021), 166324.
[28] S.U.-D. Khan, Z.A. Almutairi, O.S. Al-Zaid, S.U.-D. Khan, Development of low concentrated solar photovoltaic system with lead acid battery as storage device, Curr. Appl. Phys. 20 (2020) 582–588.
[29] S.U.-D. Khan, I. Wazeer, Z. Almutairi, M. Alanazi, Techno-economic analysis of solar photovoltaic powered electrical energy storage (EES) system, Alex. Eng. J. 61 (9) (2021) 6739–6753.
[30] Z. Lei, et al., Recent Advances of Layered-Transition Metal Oxides for Energy-Related Applications, Energy Storage Materials, 2021.
[31] A. Majid, A. Jabeen, S.U.-D. Khan, Z. Almutairi, On the prospects of layeredness in tantalum pentoxide, Mater. Sci. Eng., B 272 (2021), 115349.
[32] H. Zhang, Introduction: 2D materials chemistry, Chem. Rev. 118 (2018) 6089–6090.
[33] S.C. Pandey, X. Xu, I. Williamson, E.B. Nelson, L. Li, Electronic and vibrational properties of transition metal-oxides: comparison of GGA, GGA+ U, and hybrid approaches, Chem. Phys. Lett. 669 (2017) 1–8.
[34] S. Mandal, K. Haule, K.M. Rabe, D. Vanderbilt, Systematic beyond-DFT study of binary transition metal oxides, npj Comput. Mater. 5 (2019) 1–8.
[35] A. O'Hara, T.N. Nunley, A.B. Posadas, S. Zollner, A.A. Demkov, Electronic and optical properties of NbO2, J. Appl. Phys. 116 (2014), 213705.
[36] M. Harb, et al., Tuning the properties of visible-light-responsive tantalum (oxy) nitride photocatalysts by non-stoichiometric compositions: a first-principles viewpoint, Phys. Chem. Chem. Phys. 16 (2014) 20548–20560.
[37] S. Biswas, A DFT study of the electronic, magnetic and structural properties of rutile VO2, Proc. Natl. Acad. Sci., India, Sect. A 92 (2022) 117–128.
[38] O.K. Donaldson, K. Hattar, J.R. Trelewicz, Metastable tantalum oxide formation during the devitrification of amorphous tantalum thin films, J. Am. Ceram. Soc. 99 (2016) 3775–3783.
[39] B. Gündüz, N. Bulut, Effects of solvents on photonic and fluorescence properties of PtOEP phosphorescent material: experimental and computational analysis, J. Mol. Liq. 316 (2020), 113865.
[40] S. Garg, N. Krishnamurthy, A. Awasthi, M. Venkatraman, The O-Ta (oxygen-tantalum) system, J. Phase Equilibria Diffus. 4 (1997) 407–408.
[41] N. Schönberg, W. Overend, A. Munthe-Kaas, N. Sörensen, An x-ray investigation of the tantalum-oxygen system, Acta Chem. Scand. 8 (1954) 240–245.
[42] Y. Syono, M. Kikuchi, T. Goto, K. Fukuoka, Formation of rutile-type Ta (IV) O2 by shock reduction and cation-deficient Ta0. 8O2 by subsequent oxidation, J. Solid State Chem. 50 (1983) 133–137.
[43] Y. Muraoka, et al., Preparation of TaO2 thin films using NbO2 template layers by a pulsed laser deposition technique, Thin Solid Films 599 (2016) 125–132.
[44] U. Sahaym, M.G. Norton, Advances in the application of nanotechnology in enabling a 'hydrogen economy, J. Mater. Sci. 43 (2008) 5395–5429.
[45] C. Ravi, G. Kaur, A. Bharathi, First-principles study of lattice stability of ReO3-type hypothetical TaO3, Comput. Mater. Sci. 90 (2014) 177–181.
[46] V. Nicolosi, M. Chhowalla, M.G. Kanatzidis, M.S. Strano, J.N. Coleman, Liquid exfoliation of layered materials, Science 340 (2013).
[47] 许程, et al., Laser damage mechanisms of amorphous Ta2O5 films at 1064, 532 and 355nm in one-on-one regime, 中国物理快报: 英文版 27 (2010) 91–94.
[48] L. Zhu, J. Zhou, Z. Guo, Z. Sun, Realization of a reversible switching in TaO2 polymorphs via Peierls distortion for resistance random access memory, Appl. Phys. Lett. 106 (2015), 091903.
[49] D. Gentili, M. Gazzano, M. Melucci, D. Jones, M. Cavallini, Polymorphism as an additional functionality of materials for technological applications at surfaces and interfaces, Chem. Soc. Rev. 48 (2019) 2502–2517.

[50] A. Majid, N. Rani, S.U.-D. Khan, Z.A. Almutairi, First principles study of structural, electronic and magnetic properties of transition metals doped SiC monolayers for applications in spintronics, J. Magn. Magn Mater. 503 (2020), 166648.
[51] A. Majid, I. Ullah, K.T. Kubra, S.U.-D. Khan, S. Haider, First principles study of transition metals doped SiC for application as counter electrode in DSSC, Surf. Sci. 687 (2019) 41–47.
[52] A. Majid, K. Hussain, S.U.-D. Khan, S.U.-D. Khan, First principles study of SiC as the anode in sodium ion batteries, New J. Chem. 44 (2020) 8910–8921.
[53] A. Majid, S.A. Fatima, S.U.-D. Khan, Z.A. Almutairi, Assessment of 2H–SiC based intercalation compound for use as anode in lithium ion batteries, Ceram. Int. 46 (2020) 5297–5305.
[54] D.D. Vo, et al., Electronic structure and optical performance of PbI2/SnSe2 heterostructure, Chem. Phys. 533 (2020), 110736.
[55] A. Es-Smairi, et al., DFT Study of Structural, Electronic, Optical, and Electrical Properties of CuO Based on GGA+ U and TB-mBJ Approximations, 2021.
[56] M. Arshad Javid, et al., Structural, electronic and optical properties of LiNbO3 using GGA-PBE and TB-mBJ functionals: a DFT study, Int. J. Mod. Phys. B 32 (2018), 1850168.
[57] R.M. Almeida, A.L. da Rosa, T. Frauenheim, J.S. de Almeida, Optoelectronic properties of zinc oxide: a first-principles investigation using the Tran–Blaha modified Becke–Johnson potential, Phys. Status Solidi 256 (2019), 1800380.
[58] H. Peng, J. Li, S.-S. Li, J.-B. Xia, First-principles study on rutile TiO2 quantum dots, J. Phys. Chem. C 112 (2008) 13964–13969.
[59] G.R. Portugal, J.T. Arantes, Structural and electronic properties of NaTaO 3 cubic nanowires, Phys. Chem. Chem. Phys. 22 (2020) 7250–7258.
[60] W. Sun, W. Luo, R. Ahuja, Role of correlation and relativistic effects in MAX phases, J. Mater. Sci. 47 (2012) 7615–7620.
[61] E. Nurlaela, M. Harb, S. Del Gobbo, M. Vashishta, K. Takanabe, Combined experimental and theoretical assessments of the lattice dynamics and optoelectronics of TaON and Ta3N5, J. Solid State Chem. 229 (2015) 219–227.
[62] S. Wang, M. Jiang, L. Gao, Z. Ma, F. Wang, Theoretical and experimental studies on the crystal structure, electronic structure and optical properties of SmTaO4, Materials 9 (2016) 55.
[63] G.-S. Park, et al., In situ observation of filamentary conducting channels in an asymmetric Ta 2 O 5− x/TaO 2− x bilayer structure, Nat. Commun. 4 (2013) 1–9.